

NJC

Accepted Manuscript



This is an *Accepted Manuscript*, which has been through the Royal Society of Chemistry peer review process and has been accepted for publication.

Accepted Manuscripts are published online shortly after acceptance, before technical editing, formatting and proof reading. Using this free service, authors can make their results available to the community, in citable form, before we publish the edited article. We will replace this *Accepted Manuscript* with the edited and formatted *Advance Article* as soon as it is available.

You can find more information about *Accepted Manuscripts* in the [Information for Authors](#).

Please note that technical editing may introduce minor changes to the text and/or graphics, which may alter content. The journal's standard [Terms & Conditions](#) and the [Ethical guidelines](#) still apply. In no event shall the Royal Society of Chemistry be held responsible for any errors or omissions in this *Accepted Manuscript* or any consequences arising from the use of any information it contains.



www.rsc.org/njc

Dispersedly embedded loading of Fe₃O₄ nanoparticles into graphene nanosheets for highly efficient and recyclable removal of heavy metal ions†

Gang Zhou,^a Xiaoyong Xu,^{*ab} Wenchang Zhu,^a Bing Feng,^a and Jingguo Hu^{*a}

Received 00th,
Accepted 00th
DOI:
www.rsc.org/NJC

The regulated loading of Fe₃O₄ nanoparticles (NPs) into graphene nanosheets (NSs) matrix along with the process of reducing graphene oxide (GO) has been achieved via a facile hydrothermally self-assembling strategy. The optimized graphene/Fe₃O₄ (GF) composite with the dispersedly embedded hybridization yields high surface area serving as active adsorption sites and effective protection of Fe₃O₄ NPs against releasation, aggregation, oxidation or dissolution in wastewater, as well as the stable superparamagnetism allowing fast magnetic recycle. It exhibits a fast Cr(VI) removal with a high adsorption capacity in acidic and neutral solutions, and the adsorption kinetics following the pseudo-second-order model accords with the chemisorption in nature. Moreover, the adsorption performance shows a broad-spectrum universality to various heavy metal ions including Fe(III), Cu(II), Cd(II), etc. and has a recyclability after pH-manipulated desorption, thus the GF composite has been demonstrated as an promising separable adsorbent for removing heavy metals from wastewater.

Introduction

Heavy metal ions in the wastewater discharged from leather tanning, metallurgical manufacturing, battery production, electroplating, etc. have been regarded as a global pollutant because of their anti-biodegradation and carcinogenicity.¹ Their maximum permissible limits in drinking water and discharged industrial wastewater have been regulated by Environmental Protection Agency (EPA) in many countries.² In recent years, numbers of technologies have been developed to remove heavy metal ions from wastewater, such as ion exchange,³ reverse osmosis,⁴ electrochemical precipitation,⁵

catalytic degradation⁶ and adsorption separation.^{7,8} Among them, the adsorption separation with the practical advantages of low cost, simple process and reduced secondary pollution is a promising method suitable for the batch removal of heavy metals.⁹ Various materials including the activated carbon, zeolite, polymer and metal oxides, etc. have been demonstrated as the efficient adsorbents to purify wastewater,^{10–12} in particular, iron and iron oxide nanoparticles (NPs) have been recognized as higher effective medium for the heavy metals adsorption.^{12,13} However, the easy oxidation, rapid agglomeration and side pollution become the major challenges when using iron-based NPs adsorbents. To meet these challenges, some inert materials are usually introduced to design the matrix building for loading NPs,^{14,15} and noting that graphene or its oxide (GO) with a large dimension in XY plane and ultrahigh specific surface area is a favorable platform with great advantages in immobilizing and dispersing NPs.¹⁶ Moreover, graphene itself with a theoretical specific surface

^a School of Physics Science and Technology, Yangzhou University, Yangzhou 225002, China. E-mail: xxy@yzu.edu.cn and jghu@yzu.edu.cn

^b State Key Laboratory of Bioelectronics, Southeast University, Nanjing 210096, China

† Electronic Supplementary Information (ESI) available: [Nitrogen adsorption-desorption curves of samples, EDS and RS spectra of RGO and GF1, UV-vis absorption spectra of the Cr(VI) solution treated with GF2 at different adsorption times, UV-vis absorption spectra of the Cr(VI) solutions with different pH values before and after treated with GF2 for 20 min, as well as XRD pattern and FESEM image of the recycled GF2.]. See DOI:

area of 2630 m²/g has also received considerable attention as a highly efficient adsorbent for contaminant removal.¹⁷ Recently, the three-dimensional graphene sponges and magnetic graphene composites have been fabricated to be able to perform an easy and fast separation after absorbing contaminants.^{18,19} Furthermore, the magnetic graphene or GO hybrids could be supposed to bring about the promising progress in applications like targeted drug carriers, magnetic resonance imaging and environmental remediation based on some potential advantages, such as the large surface area for the adsorption loading and the injected magnetism for magnetic recycle and against adsorbent releasing.^{19,20} In this work, a hydrothermally self-assembling strategy was developed to synthesize the reduced graphene oxide (RGO)/Fe₃O₄ (GF) composites, in which various amounts of Fe₃O₄ NPs were incorporated in RGO nanosheets (NSs) during the reduction of GO. The tunable loading of Fe₃O₄ NPs into RGO matrix was used to explore an optimal balance between the adsorption capacity and the magnetic manipulation. The optimized GF hybrid with the dispersedly embedded assembly endows high specific surface area and stable superparamagnetism, and as a proof of concept, its removal performance of heavy metal ions was examined in terms of removal efficiency, adsorption kinetics, equilibrium adsorption capacity, pH-dependence, adsorption isotherm analysis, recycling reusability and applicable range.

Experimental

Preparation of GO

GO was synthesized by oxidizing expandable graphite powder according to the modified Hummers method.^{21,22} Typically, graphite (0.5 g), H₂SO₄ (600 mL), KMnO₄ (3 g), NaNO₃ (0.5 g) and a Teflon reactor placed into a stainless-steel autoclave were completely cooled in a refrigerator at 0–5 °C for 4.5 h. The cooled graphite, H₂SO₄, KMnO₄ and NaNO₃ were tardily poured into the Teflon reactor. Then the reactor was sealed in the stainless-steel autoclave and transferred in the refrigerator maintaining at 0–5 °C for 1 h and then heated at 80 °C in an oven for 2 h. The supernatant was removed after the autoclave was cooled naturally to room temperature. The product was diluted with 60 mL of deionized water followed by magnetic stirring for 2 h. With magnetic stirring, 5 mL of H₂O₂ was

dripped into the solution to terminate the reaction. The obtained golden yellow slurry was subsequently washed with diluted HCl solution and deionized water until the pH of the solution is larger than 5 to obtain the GO suspension. After a drying process at 60 °C for 48 h in vacuum system, the dye GO powder was obtained.

Preparation of Fe₃O₄ NPs

The Fe₃O₄ NPs were prepared by a hydrothermal method. Typically, Fe₃O₄•6H₂O (1.4 g) and CH₃COONa•3H₂O (3.5 g) were dissolved in ethylene glycol (40 ml) to form a yellow solution, followed by the addition of polyethylene glycol (1.1 g). The mixture was sonicated for 25 min and then sealed in a Teflon-lined stainless steel autoclave. The autoclave was heated and maintained at 180 °C for 10 h, then cooled down to room temperature. The black precipitates were washed several times with deionized water and dried at 50 °C in vacuum for 10 h to obtain Fe₃O₄ NPs powder.

Fabrication of GF nanocomposites

The GF heterostructures were formed by the self-assembly of RGO and Fe₃O₄ NPs along with a hydrothermal process of reducing GO. In a typical synthesis, 80 mg of GO was added into 40 mL of deionized water with sonication for 30 min to form the homogeneous GO solution. Then the as-prepared Fe₃O₄ NPs with several different mass of 10, 20, 40 and 80 mg were dispersed respectively in the above GO aqueous solution to investigate the effects of Fe₃O₄ share in the GF hybrid both on heterogeneous morphologies and on adsorption performances. After mechanical stirring for 30 min, the mixtures were sonicated for 50 min, then sealed in 50 mL Teflon-lined stainless autoclaves and maintained at 180 °C for 2 h followed by cooled naturally to room temperature. The black precipitates were thoroughly washed with ethanol and deionized water by magnetic separation, and then were dried in vacuum at 50 °C. The resulted products with four different ratios of RGO and Fe₃O₄ were synthesized, and were labeled as GF1, GF2, GF3 and GF4 with the increase of Fe₃O₄ content, respectively. In addition, the pure RGO was also prepared via the same route without the presence of Fe₃O₄ NPs.

Characterization

The X-ray diffraction (XRD) patterns of samples were collected on a Shimadzu-7000 X-ray powder diffractometer with Cu K α radiation ($\lambda = 0.15406$ nm). The morphologies of samples were characterized by using the field emission scanning electron microscopy (FESEM, Hitachi, S-4800II) equipped with X-ray energy dispersive spectrum (EDS). The Fourier transform infrared (FTIR, Varian Cary 670) and the Raman scattering (RS, Renishaw in Via) were carried out to analyse the chemical composition of composited samples. The specific surface area was measured using a nitrogen gas sorption surface area tester (3H-2000PS2, BeiShiDe Instrument S&T (Beijing) Co., Ltd.) and calculated by the Brunauer-Emmett-Teller (BET) method. The room-temperature magnetic properties of samples were measured by ADE-V7 vibrating sample magnetometer (VSM).

Adsorption experiments

Equal mass (100 mg) of six materials including pure RGO NSs, bare Fe₃O₄ NPs, and GF composites with different Fe₃O₄ contents (GF1, GF2, GF3 and GF4) were respectively put in the reagent bottle containing 0.072 mol/L of potassium dichromate aqueous solution (15 mg/L of Cr(VI)) to examine their performances of removing Cr(VI) ions. The mixture solutions were stirred under ultrasonication at room temperature for 20 min, after that, the RGO, Fe₃O₄, and GF adsorbents were separated by using a centrifuge and a portable permanent magnet, respectively. The Cr(VI) concentrations in the treated supernatant solutions were determined by colorimetric analysis based on the diphenylcarbazide method with a detection limit 5 $\mu\text{g/L}$.²³ Briefly, 5 mL of comparing solutions were taken into test tubes, then 0.25 mL 1,5-diphenyl carbazide (DPC, 5 g/L) and 0.5 mL o-phosphoric acid (4.5 M) were added. After standing for 30 min at room temperature to reach color steady, the UV-vis absorption spectra with the characteristic peaks at 540 nm denoting the remaining Cr(VI) concentrations were recorded by the JH 722S Vis spectrophotometer. Then the removal efficiency (η) of adsorbents in Cr(VI) solutions can be calculated according to the following equation:

$$\eta = (1 - C/C_0) \times 100\% \quad (1)$$

where C_0 and C are respectively the initial and remaining concentrations of Cr(VI) before and after the adsorption process, thus the lower C/C_0 denotes the higher removal efficiency (η)

or the higher adsorption efficiency of adsorbent. For the adsorption kinetics study and adsorption isotherm analysis, the relatively small amount of 10 mg adsorbent was employed to perform another slow adsorption process, in which the UV-vis absorption spectra were tracked, then the adsorption capacities (Q_t) at different time intervals were calculated according to the kinetic adsorption equation:

$$Q_t = (C_0 - C_t)V / m \quad (2)$$

where C_0 and C_t are respectively the initial and kinetic concentration of Cr(VI) in solution, V is the solution volume, m is the mass of adsorbent, and numerator term of $(C_0 - C_t)V$ denotes the kinetic adsorption amount over adsorbent. The pH effect on the adsorption performance was also investigated in wide window of pH values from 2 to 10, where the pH values of Cr(VI) solutions were adjusted by adding HCl and NaOH. Finally, to examine the practical value of the present GF adsorbent, its recyclability and applicable universality for other several typical heavy metal ions including Ni(II), Fe(III), Co(II), Cd(II), Pb(II) and Cu(II) were explored. The desorption of laden Cr(VI) was carried out by being soaked with 0.2 M NaOH solution, and the desorption efficiency was calculated based on the following equation:

$$\zeta = C_{de}V_d / mQ_c \times 100\% \quad (3)$$

where C_{de} is the Cr(VI) concentration in the eluent after desorption equilibrium, V_d is the eluent volume, Q_c is the adsorption capacity after adsorption equilibrium and m is the adsorbent mass.

Results and discussion

GO was first obtained from graphite powder by an improved Hummer's method and the Fe₃O₄ NPs were prepared by a hydrothermal method. After that the GF heterostructures were formed by the self-assembly of RGO and Fe₃O₄ NPs along with a hydrothermal process of reducing GO.

Microstructure characterization

Figs. 1(a)–(f) show respectively the FESEM images of RGO NSs, Fe₃O₄ NPs, and GF composites with different Fe₃O₄ contents (GF1, GF2, GF3 and GF4). The FESEM image in Fig. 1(a) reveals that the as-synthesized bare RGO are the two-dimensional (2D) ultrathin NSs with lamellar folding surface.

The bare Fe_3O_4 appears spherical NPs with uniform size of about 400 nm, as shown in Fig. 1(b). When introducing Fe_3O_4 NPs in the process of reducing GO, the obtained RGO NSs display many wrinkles even holes, moreover, such a surface roughness is becoming more obvious with the introduced Fe_3O_4 NPs increasing, as shown in Figs. 1(c)–(f). Obviously, the increase of wrinkled structure should be attributed to the stress induced by the attached Fe_3O_4 NPs. It is worth noting that the Fe_3O_4 NPs uniformly remain original size and well disperse in the RGO NSs matrix, where no free or aggregated Fe_3O_4 NPs can be observed. Particularly, from the insets of Figs. 1(c)–(f), it can be seen that the Fe_3O_4 NPs are not simply mixed up or blended with RGO NSs, but they are entrapped inside the surrounding of RGO NSs. Therefore, through the present hydrothermal self-assembly, i.e. that the Fe_3O_4 NPs were grafted while reducing GO, the 2D NSs help to prevent the NPs from agglomeration and simultaneously the zero-dimensional (0D) NPs act as the spacer to prevent the restacking of NSs, thus give priority to increase the specific surface area of GF composites. Basing on the N_2 adsorption-desorption isotherm analyses (Figs. S1(a)–(f)), the BET surface areas of GF composites with less than 40 mg of Fe_3O_4 NPs have indeed the significant increase relative to bare RGO NSs and Fe_3O_4 NPs, especially GF2 sample exhibits the biggest BET surface area of $109.95 \text{ m}^2/\text{g}$. In addition, the high stability of GF composites

against sonication demonstrates the strong interaction between RGO NSs and Fe_3O_4 NPs, furthermore which is resulted from unique embedded structure rather than additional molecular linkers. In fact, such an embedded hybrid format is very significant not only for improving stability of heterostructured binding to prevent the side damage of releasing Fe_3O_4 NPs but also for protecting the Fe_3O_4 NPs against oxidation/dissolution especially in acidic environment.

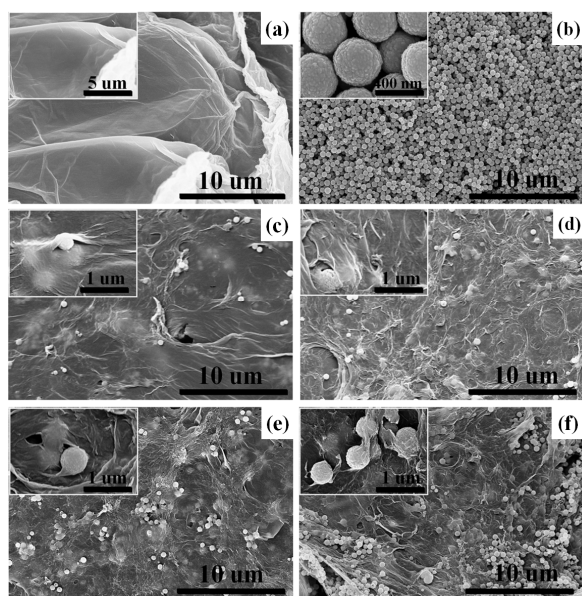


Fig. 1 FESEM images of (a) pure RGO NSs, (b) pure Fe_3O_4 NPs and hybrid GF composites with different Fe_3O_4 contents: (c) GF1, (d) GF2, (e) GF3 and (f) GF4. The insets show respectively the locally amplified FESEM images.

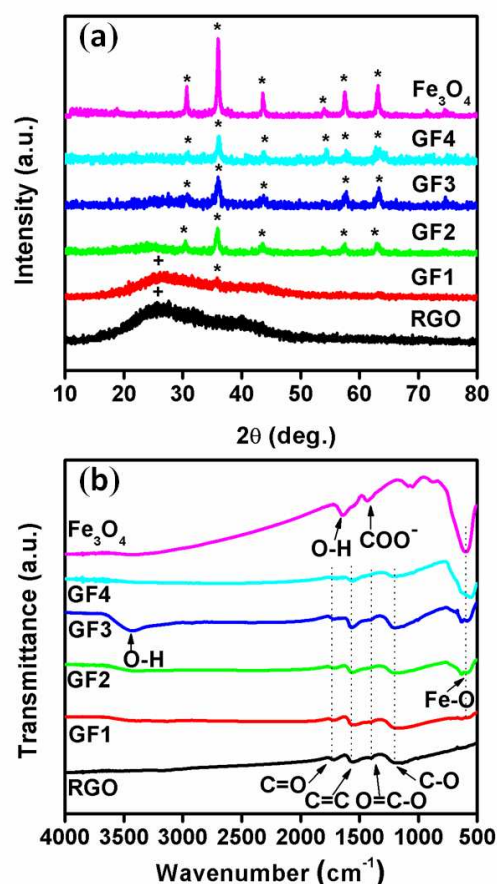


Fig. 2 (a) XRD patterns with the marked characteristic peaks: Fe_3O_4 (*) and RGO (+), and (b) FTIR spectra of hybrid GF composites with different Fe_3O_4 contents: GF1, GF2, GF3 and GF4, as well as pure RGO NSs and Fe_3O_4 NPs as two references.

To identify the chemical component of samples, the XRD, EDS, FTIR and RS spectra were collected and comparatively analyzed for the hybridized GF composites, as well as pure RGO NSs and Fe_3O_4 NPs as two references. Their power XRD patterns are presented in Fig. 2(a). The RGO shows a broad diffraction peak (+) at 25.58° , confirming the reduction of GO. With the Fe_3O_4 NPs intervening and increasing, some peaks (*) located at 30.52° , 35.92° , 43.62° , 54.08° , 57.52° and 62.94°

emerge and increase, which are found to be in good agreement with the diffraction peaks of pure Fe_3O_4 NPs and be able to be indexed respectively to (2 2 0), (3 1 1), (4 0 0), (4 2 2), (5 1 1) and (4 4 0) planes of face-centered cubic Fe_3O_4 (JCPDS No. 75-0033),¹⁹ meanwhile the RGO characteristic peak relatively weakens. The observed evolution of XRD patterns clearly indicates that the tunable incorporation of Fe_3O_4 into RGO has been achieved. Fig. 2(b) shows the corresponding evolution of FTIR spectra before and after the Fe_3O_4 NPs introducing. The bare RGO exhibits four absorption bands at 1207.22, 1390.43, 1583.27 and 1727.91 cm^{-1} , which can be assigned to the stretching modes of epoxy C–O, carboxyl O=C–O, aromatic C=C and C=O, respectively.¹⁹ As another component, the pure Fe_3O_4 NPs shows a strong absorption band at 586 cm^{-1} resulting from the stretching vibration mode of Fe–O, and other two absorption bands at 1429 and 1633.42 cm^{-1} are associated with O–H and COO^- introduced from hydrothermal preparation.^{24,25} After Fe_3O_4 NPs introduced into RGO, the absorption band of 586 cm^{-1} characterized by Fe–O vibration always appears, and its intensity increases with the added Fe_3O_4 loading, supporting further the successful incorporation of Fe_3O_4 NPs. Typically, the EDS and RS spectra of bare RGO and GF1 are compared in Figs. S2 (a) and (b), respectively. As expected, the introduced Fe element is obviously detected in the EDS spectrum of GF1, while that of RGO does not give any signal on Fe or other elements except C and O elements. The RS spectra of RGO and GF1 display two prominent peaks at 1347.28 and 1599.25 cm^{-1} , corresponding to the well-documented D and G bands of graphene. Moreover, the intensity ratio of D and G bands ($r = I_D/I_G$) is usually used as a measure of the reduction of GO, and herein the high r value of 1.03 indicates the obtaining of RGO via hydrothermal reducing GO.²⁶ Additionally, a second-order 2D band at 2684.27 cm^{-1} sensitive to the c -axis stacking order of graphene much weakly appears alone with the D+G combination band at 2939.2 cm^{-1} , indicating that the present RGO is of ultrathin tissue, being consistent with the FESEM observation. Therefore, it is conclusive that the tunable loading of Fe_3O_4 NPs into the RGO matrix in a dispersedly embedded format has been achieved in the reducing process of GO, which provides superiorities of extending the active adsorption sites and of preventing the magnetic Fe_3O_4 NPs against oxidation, dissolution or releasation for the magnetic removal of heavy metals from wastewater.

Magnetic properties

Fig. 3(a) shows the room temperature magnetic hysteresis loops of GF1, GF2, GF3, GF4, as well as bare RGO NSs and Fe_3O_4 NPs as two references. The saturation magnetizations of GF1, GF2, GF3, GF4 are of 1.03, 6.11, 18.91, 45.45 emu/g , respectively, indicating the magnetic enhancement regulated by the Fe_3O_4 NPs loading. The inset of Fig. 3(a) shows the

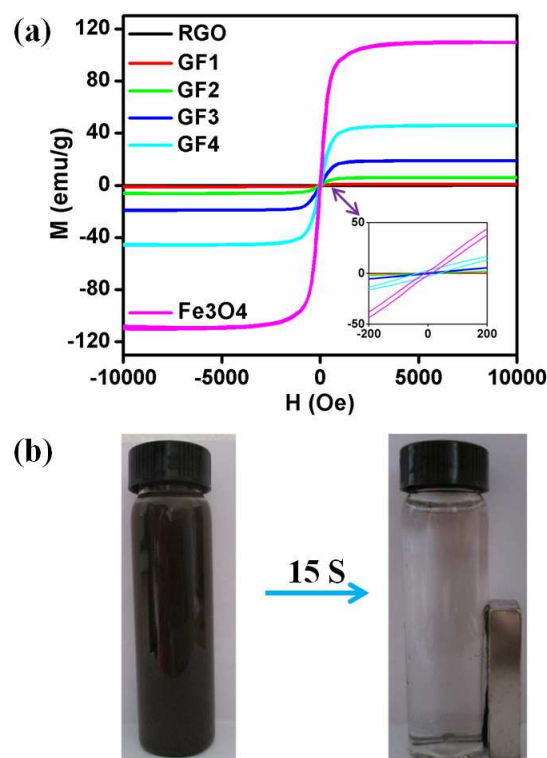


Fig. 3 (a) Room temperature magnetic hysteresis loops of hybrid GF composites with different Fe_3O_4 contents: GF1, GF2, GF3 and GF4, as well as pure RGO NSs and Fe_3O_4 NPs as two references. The inset shows the amplified centre curves. (b) Digital photographs of GF2 dispersed in water solution (4 g/L) and separated by a portable magnet within 15 s.

amplified hysteresis curves, and the GF4 with high Fe_3O_4 NPs loading exhibits an observed coercivity similar to the pure Fe_3O_4 NPs, which suggests that the close contact of Fe_3O_4 NPs may induce the interparticle dipolar interaction and the interface exchange interaction, making GF4 become ferromagnetic coupling. In contrast, the GF1, GF2 and GF3 display the superparamagnetic property without remnant magnetization and coercivity, which is valuable for the transport and separation manipulated by the applied magnetic field. Fig. 3(b) illustrates that the black GF2 dispersed in water

solution (4 g/L) can be fast separated from water by using a portable magnet within 15 s. This magnetic separation property is desirable for the recycling of nano adsorbents.

Chromium removal

The prepared potassium dichromate solution containing 15 mg/L of Cr(VI) ions were respectively treated with the equal mass (100 mg) of GF1, GF2, GF3, GF4, pure RGO NSs and

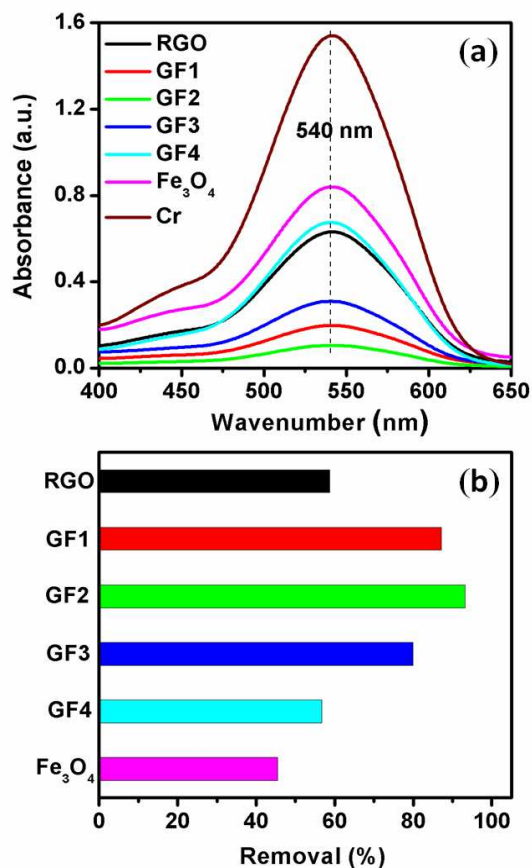


Fig. 4 (a) UV-vis adsorption spectra (a) Removal efficiencies of Cr(VI) solutions after treated with hybrid GF composites with different Fe₃O₄ contents: GF1, GF2, GF3 and GF4, as well as pure RGO NSs and Fe₃O₄ NPs.

Fe₃O₄ NPs at the room temperature to examine their removal efficiencies towards Cr(VI) ions. After treated with different adsorbents under ultrasonication for 20 min, the UV-vis absorption spectra of the colored Cr(VI) solution are shown in Fig. 4(a), and Fig. 4(b) compares their removal efficiencies at 20 min of treatment time. It can be seen that the pure Fe₃O₄ NPs and bare RGO NSs exhibit the certain adsorption capacities with the Cr(VI) removal efficiencies of about 45 and

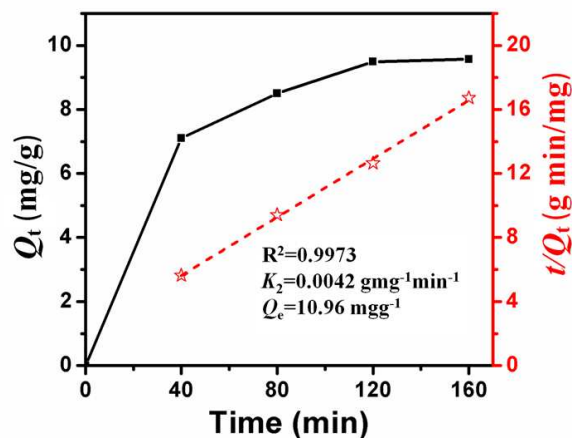


Fig. 5 Kinetic adsorption data plots of Cr(VI) over GF2: kinetic adsorption capacity Q_t vs time t (black square line) and the transformed rate plot t/Q_t vs t (red pentagram line).

59%, respectively. In comparison, the GF composites perform the obviously enhanced removal efficiencies except the GF4, and the GF2 as among the best brings out a superior removal efficiency of 94%. Obviously, such a significant increase in adsorption capacity results certainly from the integration between Fe₃O₄ and RGO, however, the superabundant addition of Fe₃O₄ can lower instead the adsorption capacity, which may be due to that the excessively Fe₃O₄ NPs loading induces more agglomeration facilitated by the increases of interparticle magnetic coupling and interfacial interaction then reduces active absorption spaces, thereby resulting in reductions of specific surface area and adsorption capacity. Such reasoning can be supported by the above characterization results of FESEM, BET and VSM. In addition, the adsorption kinetics of Cr(VI) ions over the best GF2 was explored in the designed adsorption process. The kinetic adsorption capacities calculated by equation (2) were depicted in Fig. 5, and the corresponding evolution of UV-vis absorption spectra with adsorption time are shown in Fig. S3. The adsorption kinetics was described by the pseudo-second-order model²⁷ with the kinetic rate equation expressed as:

$$dQ_t/dt = k_2(Q_e - Q_t)^2 \quad (4)$$

where Q_t and Q_e are respectively the kinetic and equilibrium adsorption capacities, k_2 is the pseudo-second-order rate constant. Integrating the equation (4) with the boundary conditions of $Q_t = 0$ at $t = 0$ and $Q_t = Q_t$ at $t = t$, the following linear form was obtained:

$$t/Q_t = 1/k_2 Q_e^2 + t/Q_e \quad (5)$$

As shown in Fig. 5, the kinetic adsorption data are fitted well to the linearized form of pseudo-second-order model with a high correlation coefficient of $R^2 = 0.9973$, and the calculated Q_e of 10.96 mg/g shows good agreement with the experimental value, moreover, it is higher than the adsorption capacities of other magnetic graphene-based adsorbents reported in some recent literatures.^{16,19} The kinetic analysis confirms further the favorable Cr(VI) adsorption over GF2, which is subject to a chemisorption mechanism behind the pseudo-second-order kinetic model.^{28,29} To examine the practical value of such a composited adsorbent in wastewater treatments, we studied further the pH dependence, the adsorption isotherm analysis, the regenerability and the compatibility for various heavy metals of the adsorption performance, typified by the best GF2.

pH effect

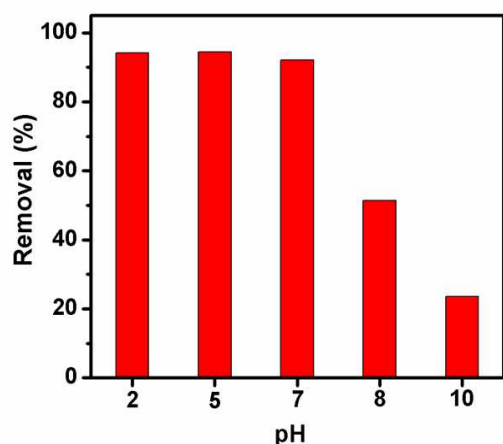


Fig. 6 Removal efficiencies of GF2 at different pH values from 2 to 10.

Since the diphenylcarbazide method itself is based on the pH-modulated colorimetric principle, the UV-vis spectra of Cr(VI) solutions with different pH values before and after adsorption treatments were recorded directly (Fig. S4) to deduce the removal efficiencies, which are shown in Fig. 6. The removal efficiencies remain almost unchanged height ($\geq 94\%$) in acidic and neutral media with the pH value range of 2–7, however, it decreases sharply in alkaline media with the PH value increasing from 7 to 10. Therefore, the GF2 adsorption capacity of Cr(VI) undergoes an observed recession in alkaline media similar to the previously reported literatures.³⁰ The

predominance diagram of the chromium species in terms of pH value and chromate concentration shows the hydrogen chromate (HCrO_4^-) is the dominant species in acidic media, while the only chromate (CrO_4^{2-}) is a stable species in alkaline media.^{31–33} As shown in Fig. S5, the UV-vis absorption spectra of untreated Cr(VI) solutions with different pH values exhibit two distinct absorption characteristics for two cases of $\text{pH} \leq 7$ and $\text{pH} > 7$, moreover, they remain respectively stable in their own pH scopes, suggesting further that the Cr(VI) exists in different ionic forms according to the watershed between the acid and alkali. Thus the pH-induced outstanding difference in removal efficiency may be attributed mainly to the varying Cr(VI) ion forms existed at different pH solutions, and the present GF2 sample may be more favorable to absorb HCrO_4^- than CrO_4^{2-} . In addition, the attachment of hydroxyl (OH^-) groups on the adsorbant surface in alkaline media can be another possible cause, which competes with the adsorption of Cr(VI) ions and leads to the decline of removal efficiency.

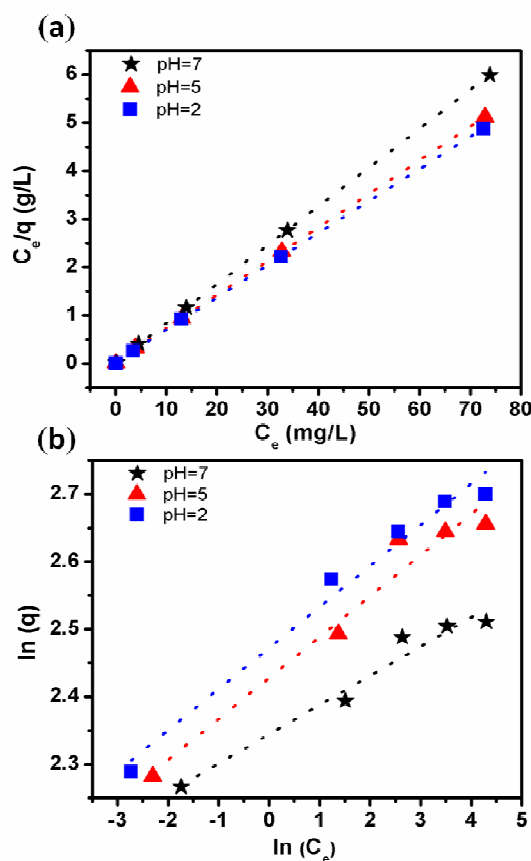


Fig. 7 (a) Langmuir and (b) Freundlich isotherms for the adsorption of Cr(VI) on GF2 at different pH values.

The partitioning of Cr(VI) at equilibrium between liquid and solid phases was modeled by Langmuir and Freundlich adsorption isotherms at room temperature under different acidic (pH=3, 5) or neutral (pH=7) environment. According to the previous literature,³⁴ the linear form of these two isotherm equations could be expressed as follows:

$$\text{Langmuir: } C_e/Q_e = 1/k_L Q_{\max} + C_e/Q_{\max} \quad (6)$$

$$\text{Freundlich: } \ln(Q_e) = \ln(k_F) + \ln(C_e)/n \quad (7)$$

where C_e and Q_e are the equilibrium concentrations of Cr(VI) in the solution and adsorbed. k_L and Q_{\max} are the constants related to the energy of adsorption and the monolayer adsorption capacity of the adsorbent. Where k_F represents the Freundlich adsorption constant and $1/n$ is the adsorption intensity. The value of k_L , Q_{\max} and k_F , $1/n$ was determined from the slopes and intercepts by plotting C_e/Q_e versus C_e , or $\ln(Q_e)$ versus $\ln(C_e)$, respectively.

After simulation, Freundlich adsorption isotherm yielded worse correlations ($R^2 < 0.98$) in description of the adsorption behavior, while Langmuir isotherm perfectly matched ($R^2 > 0.99$) and the results are shown in Fig. 7 and Table 1. This result indicates that our experimental data fits better with the Langmuir model, suggesting monolayer coverage sorption of Cr(VI) on the surface of the GF2. In addition, the calculated Q_{\max} exhibits higher value (14.95 mg/g) in acidic media than neutral media, corresponding to our previous experimental of pH effect on GF2 adsorption capacity. In a whole, in terms of both reaction rate and the adsorption capacity, GF2 demonstrated their extraordinary ability in scavenging Cr(VI) from the wastewater.

Table 1. Langmuir and Freundlich isotherm constants.

Serial no.	m/V (g/L)	PH	Langmuir constants			Freundlich constants		
			Q_{\max} (mg/g)	K_L (L/mmol)	R^2	$1/n$	K_F (mmol/g)	R^2
1	0.5	2	14.95	2.99	0.99995	0.0608	11.84	0.9725
2	0.5	5	14.30	2.51	0.99991	0.0606	11.34	0.9492
3	0.5	7	12.38	2.34	0.99988	0.0433	10.42	0.9521

Where Q_{\max} , K_L , $1/n$, K_F are defined by equations (6) and (7), respectively.

Recyclability

Fig. 8 shows the reusability of GF2 in five times of consecutive adsorption–desorption cycles. Because the adsorption of Cr(VI) over GF2 was strongly dependent on the solution pH, the desorption of Cr(VI) was carried out by using NaOH solution with an optimized concentration of 0.2 M, and about 80% of desorption efficiency could be achieved in five cycles. The

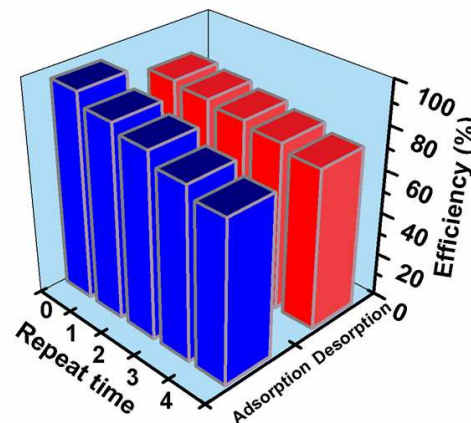


Fig. 8 Adsorption–desorption cycles of GF2.

convenient and effective desorption process endows GF2 with the certain recyclability for Cr(VI) adsorption, and the removal efficiencies maintain more than 75% along with a slight downswing, indicating that the GF2 can be facily regenerated and reused for Cr(VI) adsorption without an appreciable loss in its adsorption capacity. The structural stability of GF2 adsorbent is further confirmed by XRD and SEM for the recycled GF2 after five cycles, as shown in Fig. S6.

Other heavy metal removal

The compatibility of the GF2 adsorption property for various heavy metals was examined by treating respectively Ni(II), Fe(III), Co(II), Cd(II), Pb(II) and Cu(II) aqueous solutions with 10 mg GF2 adsorbent. As shown in Fig. 9, the measured equilibrium adsorption capacities of GF2 are 9.6, 10.1, 10.8, 9.5, 9.3 and 8.9 mg/g for Fe(III), Cu(II), Cd(II), Co(II), Pb(II) and Ni(II), which are almost at similar level with the case of removing Cr(VI). In addition, the effect of time on adsorption behavior of various heavy metals can be seen in Fig. S7. Therefore, the absorption performance of GF2 stands fairly steady towards various typical heavy metals, moreover, higher than that of some magnetite hybridized carbon-based

absorbents,^{16,35} demonstrating the present GF2 as a promising adsorbent for removal of heavy metals from the wastewater.

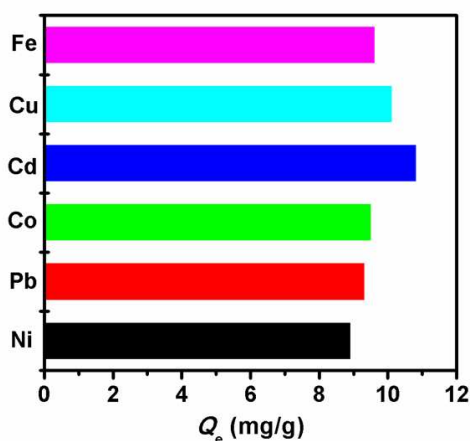


Fig. 9 Equilibrium adsorption capacities of GF2 for different heavy metal ions: Fe (III), Cu(II), Cd(II), Co(II), Pb(II) and Ni(II).

Conclusions

The reduced graphene oxide /Fe₃O₄ composites with tunable loading of Fe₃O₄ nanoparticles were fabricated by a facile hydrothermally self-assembling route, in which the various amounts of Fe₃O₄ nanoparticles were dispersedly encapsulated into reduced graphene oxide matrix. The optimized reduced graphene oxide /Fe₃O₄ (GF2) exhibited the highest specific surface area and the stable superparamagnetic property, then its fast Cr(VI) removal performance with a high adsorption capacity was demonstrated. The adsorption behavior regulated under pH value and pseudo-second-order kinetic model was illuminated as an intrinsic chemisorption. In addition, the equilibrium adsorption data were found best fit the Langmuir adsorption isotherm suggesting monolayer coverage sorption of Cr(VI) on the surface of the GF2. The superior adsorption capacity with wide applicability to various heavy metal ions and favorable renewability developed by pH-manipulated desorption suggests GF2 a promising potential for the removal of heavy metals ions from wastewater.

Acknowledgements

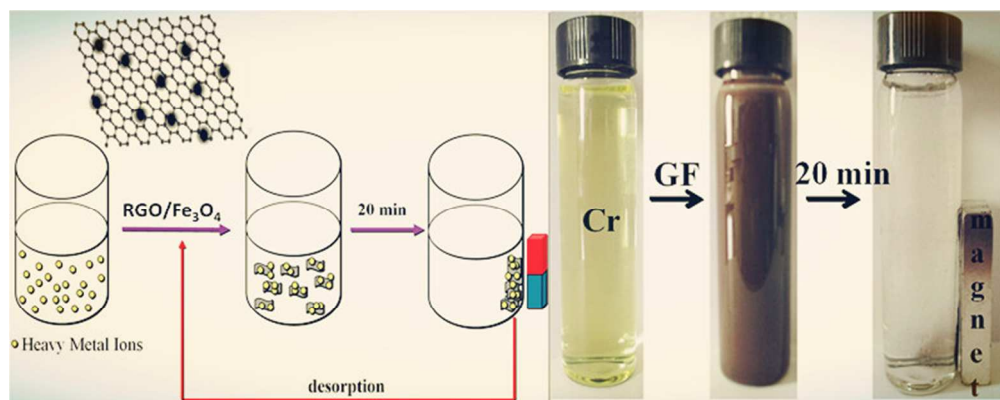
This work was supported by the National Natural Science Foundation of China (Grants 11104240, 21102135, and 11374253), the Open Research Fund of State Key Laboratory

of Bioelectronics of Southeast University and the Youth Cultivation Fund of Yangzhou University (No. 2014CXJ014). And we thank the Testing Center of Yangzhou University for the technical supports.

References

- 1 A. H. Hawari and C. N. Mulligan, *Bioresour. Technol.*, 2006, **97**, 692.
- 2 A. Baral and R. D. Engelken, *Environmental Science & Policy*, 2002, **5**, 121.
- 3 S. Rengaraj, C. K. Joo, Y. Kim and J. Yi, *J. Hazard. Mater.*, 2003, **102**, 257.
- 4 Z. Modrzejewska and W. Kaminski, *Ind. Eng. Chem. Res.*, 1999, **38**, 4946.
- 5 N. Kongsricharoern and C. Polprasert, *Water Sci. Technol.*, 1996, **34**, 109.
- 6 Y. C. Zhang, J. Li, M. Zhang and D. D. Dionysiou, *Environ. Sci. Technol.*, 2011, **45**, 9324.
- 7 D. Zhang, S. Wei, C. Kaila, X. Su, J. Wu and A. B. Karki, *Nanoscale*, 2010, **2**, 917.
- 8 Y. C. Sharma, B. Singh, A. Agrawal and C. H. Weng, *J. Hazard. Mater.*, 2008, **151**, 789.
- 9 W. Jiang, W. F. Wang, B. C. Pan, Q. X. Zhang, W. M. Zhang and L. Lv, *ACS Appl. Mater. Interfaces*, 2014, **6**, 3421.
- 10 M. A. A. Zaini, R. Okayama and M. Machida, *J. Hazard. Mater.*, 2009, **170**, 1119.
- 11 A. Chojnacki, K. Chojnacka, J. Hoffmann and H. Gorecki, *Miner. Eng.*, 2004, **17**, 933.
- 12 J. S. Hu, L. S. Zhong, W. G. Song and L. J. Wan, *Adv. Mater.*, 2008, **20**, 2977.
- 13 L. Y. Feng, M. H. Cao, X. Y. Ma, Y. S. Zhu and C. W. Hu, *J. Hazard. Mater.*, 2012, **217–218**, 439.
- 14 J. Zhu, S. Wei, N. Haldolaarachchige, D. P. Young and Z. Guo, *J. Phys. Chem. C*, 2011, **115**, 15304.
- 15 Y. J. Jin, F. Liu, M. P. Tong and Y. L. Hou, *J. Hazard. Mater.*, 2012, **227–228**, 461.
- 16 J. H. Zhu, S. Y. Wei, H. B. Gu, S. B. Rapole, Q. Wang, Z. P. Luo, N. Haldolaarachchige, D. P. Young and Z. H. Guo, *Environ. Sci. Technol.*, 2012, **46**, 977.
- 17 Z. H. Huang, X. Y. Zheng, W. Lv, M. Wang, Q. H. Yang and F. Y. Kang, *Langmuir*, 2011, **17**, 7558.
- 18 H. C. Bi, X. Xie, K. B. Yin, Y. L. Zhou, S. Wan, L. B. He, F. Xu, F. Banhart, L. T. Sun and R. S. Ruoff, *Adv. Funct. Mater.*, 2012, **22**, 4421.
- 19 V. Chandra, J. Park, Y. Chun, J. W. Lee, I. C. Hwang and K. S. Kim, *ACS Nano*, 2010, **4**, 3979.
- 20 X. Y. Li, X. L. Huang, D. P. Liu, X. Wang, S. Y. Song, L. Zhou and H. J. Zhang, *J. Phys. Chem. C*, 2011, **115**, 21567.

- 21 W. S. Hummers and R. E. Offeman, *J. Am. Chem. Soc.*, 1958, **80**, 1339.
- 22 C. L. Bao, L. Song, W. Y. Xing, B. H. Yuan, C. A. Wilkie, J. L. Huang, Y. Q. Guo and Y. Hu, *J. Mater. Chem.*, 2012, **22**, 6088.
- 23 A. Idris, N. Hassan, R. Rashid and A. F. Ngomsik, *J. Hazard. Mater.*, 2011, **186(1)**, 629.
- 24 Z. Q. Wang, D. Y. Wu, G. H. Wu, N. N. Yang and A. G. Wu, *J. Hazard. Mater.*, 2013, **244–245**, 621.
- 25 B. X. Liang, X. Wang, J. Zhuang, Y. T. Chen, D. S. Wang and Y. D. Lee, *Adv. Funct. Mater.*, 2006, **16**, 1805.
- 26 Y. H. Sang, Z. H. Zhao, J. Tian, P. Hao, H. D. Jiang and H. Liu, *Small*, 2014, **18**, 3775.
- 27 Y. S. Ho, G. McKay, D. A. J. Wase and C. F. Forster, *Adsorpt. Sci. Technol.*, 2000, **18**, 639.
- 28 G. Crini, H. N. Peindy, F. Gimbert and C. Robert, *Sep. Purif. Technol.*, 2007, **53**, 97.
- 29 Y.-S. Ho, *J. Hazard. Mater.*, 2006, **136**, 681.
- 30 X. Y. Guo, B. Du, Q. Wei, J. Yang, L. H. Hu, L. G. Yan and W. Y. Xu, *J. Hazard. Mater.*, 2014, **278**, 211.
- 31 W. J. Jiang, Q. Cai, W. Xu, M. W. Yang, D. D. Dionysiou and K. E. O'Shea, *Environ. Sci. Technol.*, 2014, **48**, 8078.
- 32 Y. Li, B. Gao, T. Wu, D. Sun, X. Li, B. Wang and F. Lu, *Water Res.*, 2009, **43**, 3067.
- 33 B. M. Weckhuysen and I. E. Wachs, *Chem. Rev.*, 1996, **96**, 3327.
- 34 Y. Li, S. M. Zhu, Q. L. Liu, Z. X. Chen, J. J. Gu, C. L. Zhu, T. Lu, D. Zhang and J. Ma, *Water Res.*, 2013, **47**, 4188.
- 35 L. Zhou, H. P. Deng, J. L. Wan, J. Shi and T. Su, *Applied Surface Science*, 2013, **283**, 1024.



TOC Graphic
282x111mm (72 x 72 DPI)